Lab on a Chip

PAPER

View Article Online
View Journal | View Issue

Cite this: *Lab Chip*, 2018, **18**, 1359

Long-term *C. elegans* immobilization enables high resolution developmental studies *in vivo*†

Simon Berger,[a] Evelyn Lattmann,[b] Tinri Aegerter-Wilmsen,[b] Michael Hengartner,[b] Alex Hajnal,[b] Andrew deMello *[a] and Xavier Casadevall i Solvas[a]

Received 7th November 2017,
Accepted 5th April 2018

DOI: 10.1039/c7lc01185g

rsc.li/loc

Live-imaging of *C. elegans* is essential for the study of conserved cellular pathways (*e.g.* EGFR/Wnt signaling) and morphogenesis *in vivo*. However, the usefulness of live imaging as a research tool has been severely limited by the need to immobilize worms prior to and during imaging. Conventionally, immobilization is achieved by employing both physical and chemical interventions. These are known to significantly affect many physiological processes, and thus limit our understanding of dynamic developmental processes. Herein we present a novel, easy-to-use microfluidic platform for the long-term immobilization of viable, normally developing *C. elegans*, compatible with image acquisition at high resolution, thereby overcoming the limitations associated with conventional worm immobilization. The capabilities of the platform are demonstrated through the continuous assessment of anchor cell (AC) invasion and distal tip cell (DTC) migration in larval *C. elegans* and germ cell apoptosis in adult *C. elegans in vivo* for the first time.

Introduction

Given its small size, fecundity and transparency the nematode *Caenorhabditis elegans* is one of the most powerful model organisms in modern biology. *C. elegans* has been used extensively to study a broad variety of biological processes, ranging from whole animal aging and stress responses[1] to development at both cellular[2,3] and subcellular resolution.[4,5]

However, many studies require worms to be immobilized prior to imaging, since animal movement greatly interferes with data acquisition. Conventionally, immobilization is achieved by "padding" worms on agar slabs[2,3] which is further improved through the administration of tranquilizing drugs.[6,7] Whilst simple and effective in suppressing movement, the use of agar pads and, more importantly, of tranquilizing drugs, significantly affects, or even terminates, many sensitive processes of interest. Such is the case for germ cell development, which cannot be studied continuously *in vivo*, since immobilization causes rapid arrest of all germline processes.[8]

In recent years, a number of microfluidic platforms have emerged enabling the efficient trapping and immobilization of single worms. The elegant work of Guo *et al.*[9] demonstrated that immobilization using a microfluidic device could be achieved to such an extent, that single neurons could be identified and severed using a femtosecond laser, and nerve regeneration studies performed. Similarly, Chung *et al.*[10] demonstrated high-throughput, high-resolution image based screening and sorting of worms using an automated microfluidic platform. While expedient for their applications, these immobilization approaches, like many others, exert considerable disruptive forces on the immobilized worm, including pressure[9–14] and temperature.[11,15] Unsurprisingly, these methods are therefore unsuited for the *in vivo* study of dynamic cellular processes over extended periods of time. Alternative approaches have been developed that allow for the maintenance of worms over longer periods of time, in the range of hours to days. This is either achieved by loosely or temporarily confining single worms[16] or by simply keeping worms unrestricted in large chambers[17–21] thus minimizing any strain imposed by the microfluidic device. For instance, the platform developed by Kopito *et al.*[16] allows gentle trapping of adult worms for up to 16 hours, maintaining normal feeding and egg laying, and facilitating the study of stress response and physiological processes. However, motion of the worm within such a trap prohibits any imaging at high magnification, thus rendering tracking of dynamic cellular processes impossible. Recently Gritti *et al.*[18] proposed a different approach for long-term imaging by simply confining *C. elegans* larvae in small chambers. Unrestricted animals could be imaged at high frame-rates, thus reducing the effects of animal motion. Such a methodology yielded relatively high-resolution images, with larval development being studied over the course of several days at the cellular level. Whilst

[a] *Institute of Chemical and Bioengineering, ETH Zurich, 8093 Zurich, Switzerland. E-mail: andrew.demello@chem.ethz.ch*
[b] *Institute of Molecular Life Sciences, University of Zurich, 8057 Zurich, Switzerland*
† Electronic supplementary information (ESI) available. See DOI: 10.1039/c7lc01185g

being one of the most advanced implementations of high-resolution imaging and long-term viability so far, this approach still poses considerable limitations on the microscopy equipment (limited to 40× magnification) and imaging technique (limited to epifluorescence and brightfield microscopy) due to the need for high acquisition frame-rates, short exposure times (between 1 and 10 ms) and bright fluorescent markers. Keil *et al.*[21] showed a modification of this approach employing trap chambers covered by a large inflatable membrane, thus allowing worms to move freely for the majority of the experiment, only immobilizing them during imaging. This removes limitations on magnification, fluorescent markers and acquisition speed, while still yielding excellent long-term viability. However, in both cases worms are imaged in random positions and orientations, limiting these approaches to the study of easily traceable processes, meaning that tracking complex spatiotemporal processes remains intractable. Study of adult animals is further complicated, as eggs cannot easily be removed from the trap chambers. To conclude, there is no system to date that allows long-term imaging of complex and sensitive dynamic processes with high resolution, except under very specific conditions.

To address such limitations, we describe a novel platform (Fig. 1a) that allows for both, long-term immobilization of normally developing animals, as well as high-resolution imaging and tracking of complex biological processes (Fig. 3a and b, 4b and c and 5a), all using a simple to use, inexpensive microfluidic device. The capabilities of the platform are demonstrated by monitoring distal tip cell (DTC) migration and anchor cell (AC) invasion in larval *C. elegans* and germ cell apoptosis in adult *C. elegans*; three processes significantly affected by conventional immobilization, with the latter two having been to date impossible to study under physiological conditions *in vivo*. We further give detailed protocols describing device fabrication and operation, so as to showcase its ease of use and facilitate adoption of the methodology by non-specialized research groups.

Results

Device fabrication and setup.

The microfluidic device was fabricated using soft lithographic methods.[22] Briefly, a master mold was fabricated *via* standard photolithography. A 50 μm thick resist layer (SU-8 3050, Microchem, Germany) was used to fabricate the adult traps. Traps for L3 and L4 larvae were 15 μm and 20 μm thick, respectively (SU-8 2010, Microchem, Germany). All masters were treated with chlorotrimethylsilane (Sigma Aldrich, Switzerland) vapour in a vacuum desiccator to prevent adhesion of PDMS during molding and demolding.

The microfluidic device was fabricated from polydimethylsiloxane (PDMS, Sylgard 184 A : B, 20 : 1, Dow Corning), cured overnight at 70 °C, peeled off the master and access holes (Gauge 20) punched. Finally, the structured PDMS slab was bonded to a cover slip (#1.5 cover slip 24 × 40 mm, ThermoScientific, Switzerland) after air plasma treatment, and stored at 70 °C overnight, to ensure complete bonding.

On-chip viability and imaging of adult hermaphrodites

Achieving long-term viability of immobilized *C. elegans* has proven difficult due to the need to feed and maintain normal bodily functions, as well as the general sensitivity of the worm to external factors. This is especially true in the case of adult hermaphrodites, where additional complications arise due to egg laying. Egg laying is readily inhibited by environmental factors or physical obstruction, resulting in termination of all germline-related developmental processes and the worm's death within a few hours.[23] Care must therefore be taken when designing the immobilization device, ensuring that all physiological needs are accommodated.

In our microfluidic device, optimal immobilization is achieved by carefully adjusting the trap channel geometry to the size and shape of the worm. Following this principle all worm motion is kept to a minimum. Immobilization is further improved by using two on-chip hydraulic valves. A set of small pillars is positioned alongside the vulva to permit unencumbered egg laying. Application of pressure is required to maintain the position of the worm and minimize its movement. However, excessive pressure, especially when applied to the vulva, leads to the termination of many developmental processes and ultimately death, a fact readily observed when using agar pads. The immobilization device was therefore optimized, so that animals are held firmly enough to permit high resolution imaging, whilst allowing minimal motion originating from the pharynx, intestine and gonad, necessary for normal physiological function and development. Additional channels positioned along the main trap allow constant supply of a bacteria suspension, ensuring that the immobilized worms are sufficiently fed (Fig. 1a and Fig. S1A†).

The performance of the immobilization platform was validated using two criteria: motion and egg laying. We found that inside the microfluidic device adult worms regularly survive for approximately 100 hours (95 h ± 21 h, n = 9), and in exceptional cases for up to 170 hours (Fig. 1f). This surpasses lifespans achieved in previously reported microfluidic traps by one order of magnitude[16] and in conventional immobilization techniques by twenty-fold.[8] To further assess the effect of immobilization on viability and health, we performed comparisons with worms kept on-chip but in larger chambers (650 × 300 × 50 μm, $L \times W \times H$), and therefore able to crawl freely. These worms showed very similar survival (111 ± 19 h, n = 3), indicating that our immobilization strategy does not affect survival in a significant way (Fig. 1g and Fig. S1C†). Under unfavourable conditions, *e.g.* insufficient food supply, unfavourable chemical environment or excessive amounts of pressure, egg laying is immediately halted. When using conventional agar pads, very few ovulations occur and generally no egg laying is observed. Significantly, within the microfluidic immobilization device egg laying occurs at an average

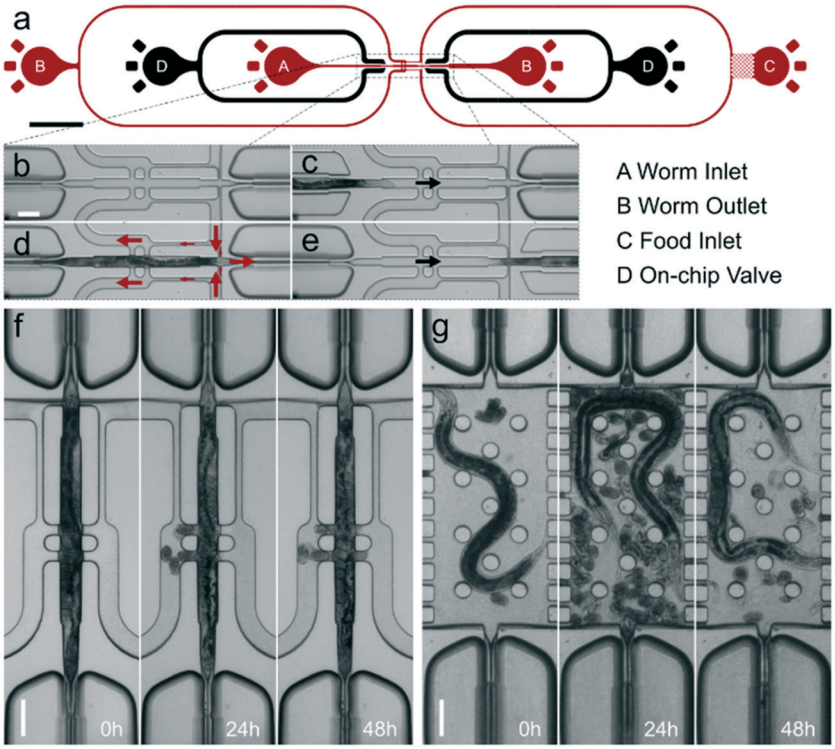

Fig. 1 Schematic of the device and its operation. (a) Schematic of the adult *C. elegans* immobilization device. Fluidic channels are marked in red, on-chip valves in black. Gentle immobilization and long-term viability are achieved using three on-chip operations. First, loading and isolation are achieved and controlled through two sets of on-chip valves (black), placed alongside the main channel. Second, the immobilization section is designed to perfectly match the worm's body. Third, bacteria are continuously supplied to the worm, allowing it to feed normally and maintain normal body functions. (b–e) Worm loading (Movie S1†). (b) Empty chamber. (c) Worm enters. First on-chip valve is open, second on chip valve remains closed preventing the worm from leaving the chamber. (d) Immobilized worm. Both on-chip valves are closed. (e) If a worm is unsuitable for an experiment, the second valve is opened and the worm released. (c–e) Arrows indicate major flow directions during loading (black) and immobilization (red). (d) Importantly the bacteria flow is not affected by the closed valve, as the channel is not completely blocked. A significant portion of the bacteria flow is permanently directed to the worm's head, through the closed valve to outlet B. (f) Single adult *C. elegans* immobilized on chip. Images, from left to right, show the worm at 0 h, 24 h and 48 h (Movie S2 and S5†). (g) Comparison with a worm kept on-chip, but in a non-immobilized state. In both cases the worms are healthy, and behave normally. Scale bar 1000 μm (a) and 100 μm (b–g).

rate of 1 egg every 15 minutes (176 ± 17 eggs in 48 h, n = 7), a rate consistent with on-plate observations (176 ± 30 eggs in 48 h, n = 10). Hence, our results suggest that viability within our microfluidic device is optimal, observing no negative effects on feeding, egg laying and general development (Movie S2†). Overall, the microfluidic immobilization device showed very reliable performance, provided that the bacteria density is well matched, no clogging or change in bacteria concentration is observed over the entire duration of the experiment. Likewise, no obstruction of egg laying by the microstructures was observed, and eggs are reliably washed out of the device after laying, such that no channel clogging and associated negative effects on the immobilized worm are observed.

Equally important to worm viability is the immobilization performance and the resulting image quality achievable when using the microfluidic device. Excessive animal motion or rotation will greatly interfere with data acquisition, rendering high-resolution imaging and tracking of complex dynamic processes impossible. We illustrate the compatibility of our immobilization device using three commonly used imaging modalities, epi-fluorescence (EPI), spinning disc confocal (SDC) and differential interference contrast (DIC) microscopy, acquiring z-stacks of the gonad of adult hermaphrodites and comparing the image quality obtained to images acquired on agar pads (Fig. 2a–f and Fig. S3†). Worms can be imaged at high resolution within the microfluidic device, using a high magnification, high numerical aperture objective (60× water immersion, NA 1.2), owing to the fact that PDMS is transparent and directly mounted on a thin cover slip. Importantly, no bodily rotation is observed during the experiments, with movement within a z-stack and between time intervals remaining minimal. Use of the microfluidic device did not alter image quality or long-term photostability, nor did it require any modification to established imaging protocols. The device could readily be mounted on different microscopes and excellent quality images were acquired using all assessed imaging modalities. Accordingly, data quality and resolution is limited solely by the imaging technique chosen. Notably, contrary to agar pads, very little drift is observed during imaging, with only a 1–3 μm drift during a 12 hour imaging session. Expensive autofocusing units, or manual drift correction are therefore unnecessary.

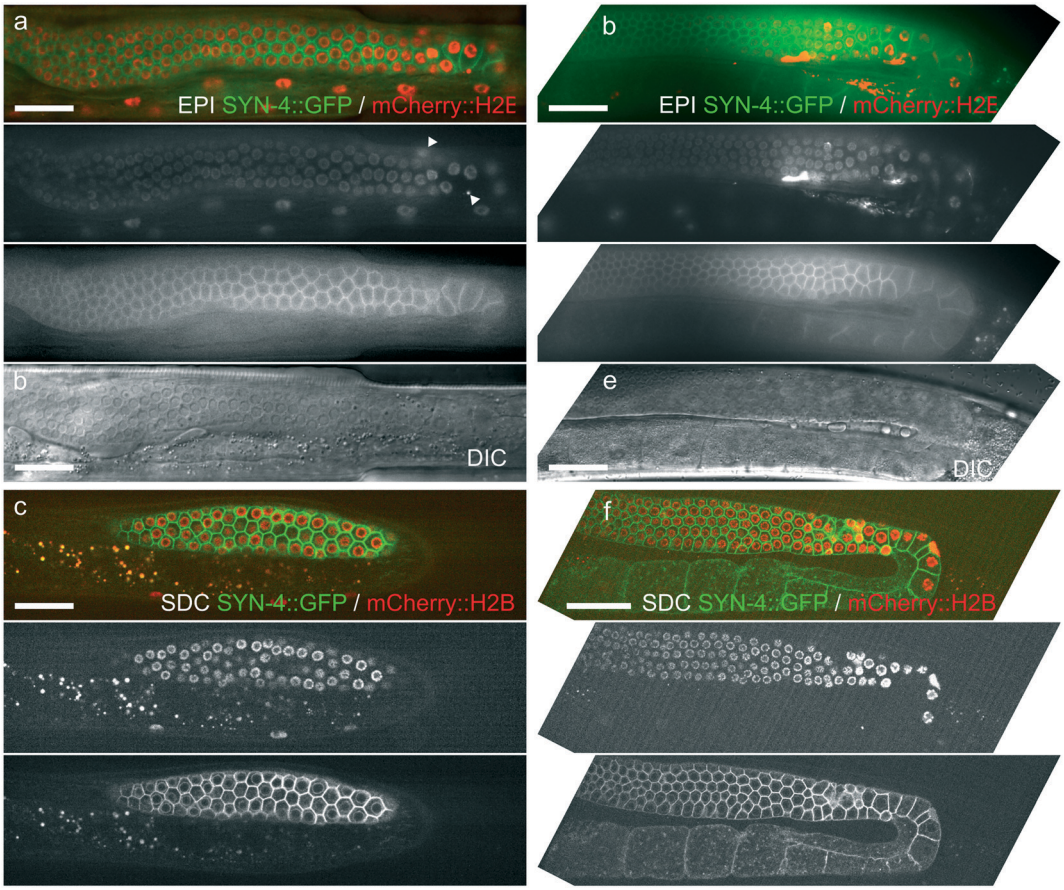

Fig. 2 Representative images of the germ cells in adult *C. elegans*. (a–c) Images acquired on-chip, (d and e) images acquired on agar pads. (a and d) Epi-fluorescence, (c and f) spinning disk confocal imaging. For both overlay, and separate fluorescence channels are shown (mCherry, GFP). (b and e) DIC microscopy. All three imaging modalities show excellent compatibility with the developed platform. No difference in image quality between images acquired on-chip or on conventionally used agar pads is visible. (a) Apoptotic cells are indicated by arrows. Images acquired using a 60× objective (NA 1.2). Scale bar 25 μm.

Germ cell apoptosis and cell fate tracking

Programmed cell death is a ubiquitous process in metazoan development. *C. elegans* has been instrumental in elucidating the regulation that underlies this process and several genes important for apoptosis in higher organisms were initially identified in worms.[24–26] Germ cells migrate along the gonad of adult hermaphrodite *C. elegans* in a temporally ordered manner. Once the germ cells exit the pachytene stage of meiotic prophase I they either enter diakinesis, and differentiate into oocytes, or undergo apoptosis.[27–29] Germ cell apoptosis is essential to maintain cellular homeostasis in the gonad and prevent the overproduction of costly oocytes under unfavourable conditions. The process can be readily visualized under a microscope owing to the optical transparency of *C. elegans*. While much progress has been made in understanding the regulation of germ cell apoptosis in *C. elegans*, several questions, such as the identity of dying cells, as well as the factors triggering apoptosis, remain unanswered. Many of these questions may be answered by simply following germ cells during their migration along the gonad arms and analysing potential factors that may lead to the apoptotic cell fate. However, while simple in theory, the long time periods over which germ cell migration occurs and the shortcomings of existing immobilization techniques, resulting in the arrest of the sensitive germline processes within 20–30 minutes,[8] have severely impeded our understanding of germ cell apoptosis dynamics. Commonly, germ cell apoptosis is assessed by padding worms on glass slides, determining the occurrence and number of cell corpses at any given time. Knowing the number of cell corpses and the fact that cell corpses usually do not remain in the gonad for extended periods of time, allows rough estimates of the rate at which apoptosis occurs. Alternatively, by measuring egg laying rates and mitotic rates, determined by staining the mitotic spindle in fixed animals, apoptotic rates can be inferred. It is generally estimated that between 50% and 80% of germ cells die upon exit from the pachytene[27,30,31] However, while these approaches give semi-quantitative information on the occurrence of apoptosis, no additional information can be obtained (such as the time leading up to the cell fate decision and involved factors). Such information can only be gained by tracking germ cell migration *in vivo*. It is important to note that extrapolating mitotic rates from fixed animals can result in large errors;

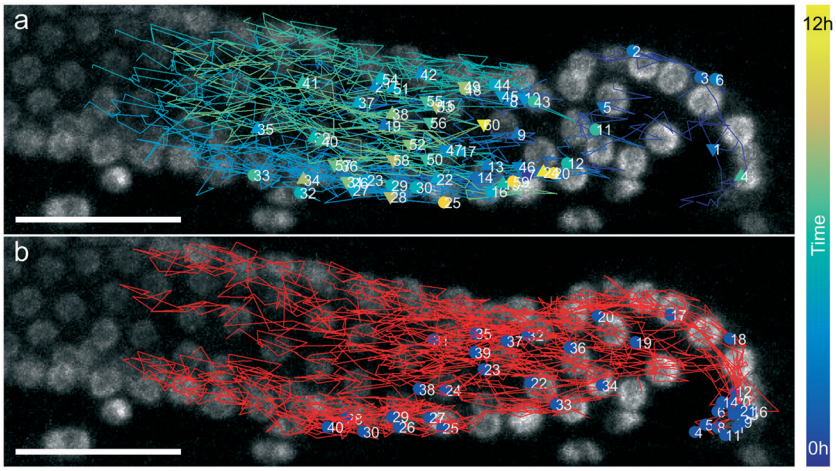

Fig. 3 Germ cell tracking. (a and b) Cell tracking within the gonad over the course of 12 hours. 100 cells were tracked, 60 of which underwent apoptosis. The majority of cells die just prior to the turn of the gonad (a). The remainder of cells did not show signs of apoptosis within the timeframe of the experiment (b). Cell tracks are overlaid on a maximum intensity projection of the first acquired Z-stack. Colors in (a) indicate the time at which cells entered the region of interest. Circular and triangular markers indicate the section from which the germ cells originate. Circular indicates the midsection of the gonad, triangle up and triangle down indicate the upper and lower section respectively. Cells can therefore be tracked in 3D over extended periods of time. Scale bars 25 μm.

likewise, the extrapolation from cell corpses to apoptotic rates is highly error prone.

Therefore, after ensuring that our microfluidic device delivers optimal immobilization and long-term viability, we used it to dynamically record and study germ cell migration and apoptosis *in vivo* for the first time (Movie S3†). We visualize the germ cells in the *itIs37[pie-1p::mCherry::H2B]; xnIs87[syn-4p::GFP]* strain, that expresses fluorescently labelled histone and t-SNARE transgenes to identify the germ cell nuclei and cell membranes respectively. Apoptosis is indicated by both the observation of engulfment and the associated disappearance of the cell membrane marker, accompanied by a sharp increase in nucleus fluorescence intensity (Fig. 2a). This increase in fluorescence intensity stems from the degeneration of the nucleus during apoptosis and correlates well with the occurrence of cell corpses observed in DIC.

Using our platform, we were able to intimately track individual germ cells over extended periods of time and quantify the rate at which apoptotic cell fates occur directly *in vivo*. We tracked cells in three worms (n_1 = 100 cells, n_2 and n_3 = 20 cells) which were continuously imaged for a period of 12 h. We found apoptotic rates of 60% in the first two animals and of 85% in the third one and an average cell migration rate in the first worm of 3.11 μm h^{-1} (Fig. 3a and b and Fig. S4†). In addition to determining apoptotic rates directly, we could analyse how germ cells migrate along this part of the gonad. For this we divided the images acquired into small rectangular cuboids and scored the frequency at which cells are present in each of these cuboids, accumulated over time (colour coded in Fig. S4A–D†). This data was then used to generate transverse plots by summing up values along the left–right (Fig. S4A and B†) and proximo-distal (Fig. S4C and D†) directions, resulting in a representation of the distribution of cell fates and cell migration patterns along the gonad. From these plots, it appears that germ cells are not uniformly distributed throughout the gonad, but are most frequently found passing through small sections on the dorsal and ventral side of the gonad, as well as to a lesser extent on the left lateral side of the gonad. Apoptotic fates appear more frequent on the ventral side (Fig. S4A and C†), while non-apoptotic fates are more commonly found on the dorsal side (Fig. S4B and D†). In the plots generated in the left–right direction, these sections can be seen right before the gonad's turn. Plots for apoptotic fates alone (Fig. S4A†) show a discontinuity at the entrance of the turn, while non-apoptotic fates (Fig. S4B†) appear to be continuously distributed along the length of the gonad.

Given the non-uniform distributions of apoptotic cells and non-apoptotic cell fates, a correlation between the initial position within a distal cross section and the final cell fates seemed likely. When examining the distribution of germ cells along the proximo-distal axis more closely (Fig. S4E†) though, this appears not to be the case and both eventual cell fates are evenly distributed along the circumference of the gonad at the distal side. Only very close to the turn this distribution becomes biased to the ventral side for apoptosing cells (yellow) and to the dorsal side for non-apoptosing cells (blue). Evidently, close to the turn the gonad undergoes significant geometrical rearrangement, turning from its original tube-like structure into a denser one, with a constriction allowing cell passage into the turn only close to the right side (Fig. S4A, B and E†). This structural rearrangement implies that cells originally migrating on the ventral side cannot directly enter the turn of the gonad, unless they first migrate towards the dorsal side. Cell fate thus appears to be determined at a stage with considerable migration between the dorsal and ventral side of the gonad.

Adaptation for larvae immobilization

C. elegans development is divided into four larval stages, L1–L4. Many of the processes occurring during larval development are highly dynamic, making them ideally suited for time-lapse live-imaging. However, immobilization on agar pads, severely disrupts larval developmental and its dynamics. For this reason, we adapted the same strategy demonstrated for adult *C. elegans*, developing a set of immobilization devices for both L3 and L4 stage larvae (Fig. 4a and Fig. S1B†). The setup process, operation, and performance (high resolution, high magnification imaging and compatibility) of the larvae immobilization device are identical to those for the adult device.

Larval viability on-chip was determined by assessing the minute motion possible within the trap (*i.e.* twitching and feeding) as well as the occurrence and dynamics of developmental processes. We found that larvae immobilized in our devices showed normal behaviour and development (Fig. 4b–e, 5a and Fig. S5†). Larvae were regularly immobilized for 12 hours. Longer immobilization was not tested as molting is not possible on-chip and developmental arrest occurs at the L3/L4 or L4/adult molt. In order to get more elaborate information about developmental dynamics on-chip, we studied two processes in more detail, DTC migration and anchor cell invasion.

Distal tip cell migration (DTC)

DTC migration begins in the L1 stage and ends during the L4 stage. It essentially guides and defines the shape of the *C. elegans* gonad. During the L2 and L3 stages, the DTCs migrate outwards in anterior–posterior direction, turning from the ventral to the dorsal side by the end of the L3 stage. Migration towards the body center is observed during the L4 stage. Thus, DTC migration is an essential and highly dynamic process that serves as a good indicator of whether larval development occurs normally.[5,32,33]

DTC migration has been extensively studied using agar pads and tranquilizing drugs, which significantly affect the rate at which this process occurs. We assessed the developmental rates of DTC migration in worms immobilized on agar pads with 4 mM Tetramisole and in free crawling worms on NGM plates, and compared it to rates measured on-chip.

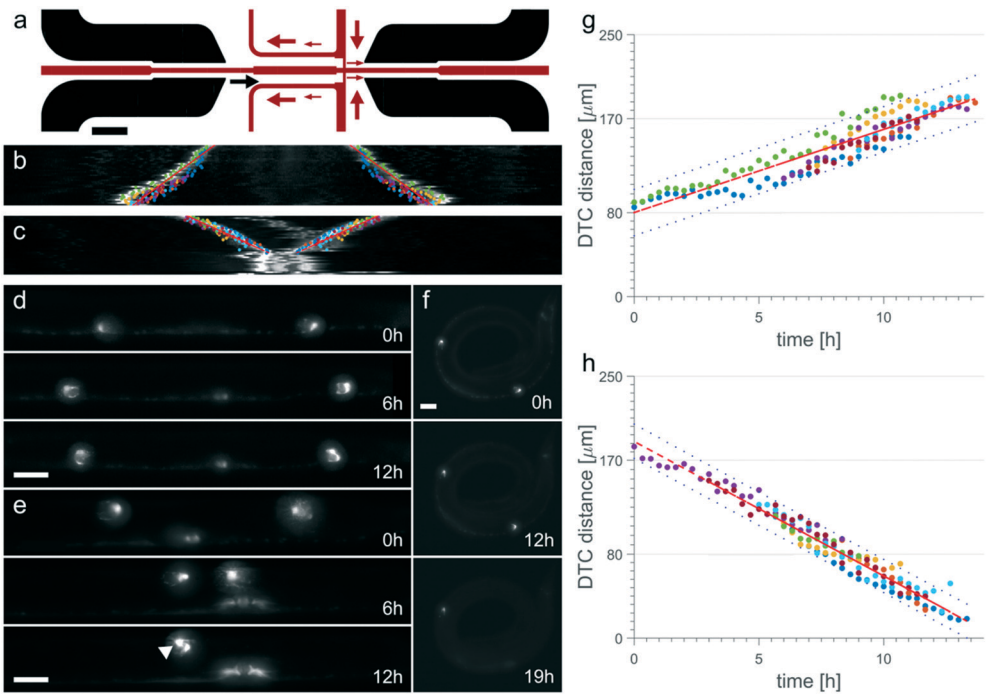

Fig. 4 Larvae immobilization and DTC migration. (a) Schematic of the larvae immobilization device. Compared to the adult device all channel dimensions have been adjusted to house the smaller larvae. Arrow indicate major flow directions during loading (black) and immobilization (red). (b and c) Kymograph depicting on-chip DTC migration in anterior posterior direction, during L3 and L4 stage. Both the outward growth and turn during L3 stage (b) as well as the growth towards the body centre during L4 stage (b) are observed to progress normally (Fig. S5 and S6†). Each line of the kymograph corresponds to a single time point (ranging 0–12 h), overlaid are the DTC positions during multiple experiments. (d–f) Comparison DTC migration on-chip and on agar pads. Maximum intensity projections depicting DTC migration in L3 larvae immobilized on-chip (d). Maximum intensity projections depicting DTC migration in L4 larvae immobilized on-chip (e). The normal migration path is observed for both L3 and L4 larvae. Equal image quality is obtained as on agar pads. Triangle indicates DTCs. (f) However, DTC migration does not happen or only to a limited extent on agar pads. Typically, after long immobilization times damage to the immobilized larva is observed, resulting in shrinkage of the worm or disappearance of the DTC. (g and h) Linear regression of on-chip DTC migration. Represented is the distance between the DTCs as a function of time, resulting in a growth rate of 7.96 ± 0.25 μm h^{-1} in L3 (g) and 12.87 ± 0.23 μm h^{-1} in L4 (h). Each colour represents a separate worm. Images acquired using a 40× air immersion objective (NA 0.6). Scale bar 100 μm (a), 25 μm (b–f).

DTC migration was visualized in *qIs56[lag-2p::GFP]* animals, where the DTC is fluorescently labelled. On agar pads we observed growth rates for L3 of 3.40 ± 0.6 2 μm h^{-1} (n = 2), compared to the 11.19 ± 2.24 μm h^{-1} for L3 (n = 4) and 12.15 ± 1.84 μm h^{-1} for L4 larvae (n = 6) freely crawling on NGM plates (Fig. S6C and D†). Crucially, only two out of the seven L3 animals imaged on agar pads displayed DTC migration in the anterior–posterior direction; furthermore, migration was incomplete. In the remaining five larvae DTC migration did not occur at all (which we expect to be the case for L4 as well). Additionally, shrinkage of the worms or damage to the animal was often observed when immobilizing worms on agar pads.

By comparison, we found that within the microfluidic device DTC migration occurs normally and at rates comparable to free crawling worms on NGM plates. Both the outward growth and turn during the L3 stage (Fig. 4b and 3d), as well as the growth towards the body center during the L4 stage (Fig. 4c and 3e) are observed to progress normally on-chip. We found growth rates of 7.96 ± 0.25 μm h^{-1} and 12.87 ± 0.23 μm h^{-1} for L3 and L4 larvae respectively (n = 7) (Fig. 4g and h, Fig. S5 and S6A and B†).

Both the drastic decrease in developmental rate as well as the morphological changes apparent when using agar pads, most likely stem from a lack of food as well as the adverse effects of Tetramisole, a paralyzing agent (Fig. 4f). DTC migration on-chip occurred in all animals studied (n = 14) with no apparent morphological changes, yielding migration rates comparable to free crawling worms on NGM plates, indicating that development is not significantly affected by our immobilization technique. Differences in growth rates on-chip and on plate most likely stem from less accurate measurements on plate, caused by the lower image quality obtainable as well as the worms actively contracting and stretching while moving on the plate. Additionally a slight decrease in growth rate might stem from the immobilization on-chip, since immobilization inherently interferes with the worm's natural growth.

Anchor cell (AC) invasion at the subcellular level

Finally, we used our platform's ability to follow subcellular processes dynamically and under physiological conditions to observe cell invasion in real-time. Cell invasion, a process whereby cells attach to, breach and migrate through basement membranes, plays a central role in many developmental processes, *e.g.* angiogenesis and organogenesis. During the L3 stage of *C. elegans* development, the anchor cell, a specialized cell of the uterus, undergoes such an invasion, by which the uterine and vulval tissue are connected. Since the anchor cell and the underlying basement membranes can easily be labeled with fluorescent markers, this process represents an ideal model for the study of cell invasion mechanisms,[34–36] furthermore representing a process similar to epithelial–mesenchymal transition in vertebrates.[37]

While much is already known about anchor cell invasion, live-imaging of the entire process in natural as well as perturbed conditions (*i.e.* RNAi/drug treatments) has not been done routinely, but would undoubtedly increase our understanding of this dynamic invasion process. So far, real time observations have been complicated by the shortcomings of conventional imaging techniques, as immobilization and high-resolution imaging are requisite. Immobilization is regularly achieved using agar pads in combination with tranquilizing drugs (*e.g.* tetramisole), which has significant detrimental effects on the dynamics of this process. Alternatively, time-lapse imaging or images of multiple animals at different points in the development can be acquired, reconstructing the process from multiple time points and animals. This approach, however, is laborious and exact information about developmental timing can only be obtained with considerable difficulty. We therefore applied our microfluidic immobilization method for the study of AC invasion in L3 larvae.

We visualized AC invasion in *qyIs23[cdh-3p::mCherry]*; *qyIs10[lam-1p::lam-1::GFP]* animals, where both the actin in the AC and the basement membrane are fluorescently labelled. The faint signals and small details of this reporter system, such as the opening in the basement membrane formed during the invasion process, demand the use of high numerical aperture, high magnification objectives and thus efficient immobilization. Especially during early L3 stage, the *qyIs23[cdh-3p::mCherry]* marker is very faint, resulting in very low signal and grainy character of the images obtained (Fig. 5b).

We observed actin dynamics within the AC and the formation of an opening in the basement membrane dynamically, in high resolution and under physiological conditions, a feat previously not possible. On average, AC invasion occurred within 1.62 ± 0.65 hours on-chip (n = 7) (Fig. 5a and b and Movie S4†), which is in excellent agreement with the timing assumed for free crawling worms. When compared to traditional immobilization on agar pads, our on-chip strategy delivers the same image quality and comparable immobilization performance, yet AC invasion is not obstructed on-chip. Within the microfluidic device all worms tested underwent AC invasion, and no complications were observed during the larvae experiments. By comparison, on agar pads with 4 mM tetramisol only 25% of worms underwent AC invasion (n = 8). Similarly, AC invasion on agar pads typically required 5–7 hours (n = 2) (Fig. 5c). The drastic decline (or even arrest) of this developmental process on agar pads is almost certainly due to the adverse effect of the drug as well as the lack of a constant food supply. It should further be noted that when using agar pads the lumen is usually not as well defined, with the process terminating immediately after the opening in the basement membrane is formed. This is most likely a result of long immobilization times. On-chip, the lumen was fully formed after 3.75 ± 0.75 h. This further confirms that our gentle, reagentless immobilization procedure is uniquely suited for the unhindered *in vivo* study of developmental processes under physiological conditions.

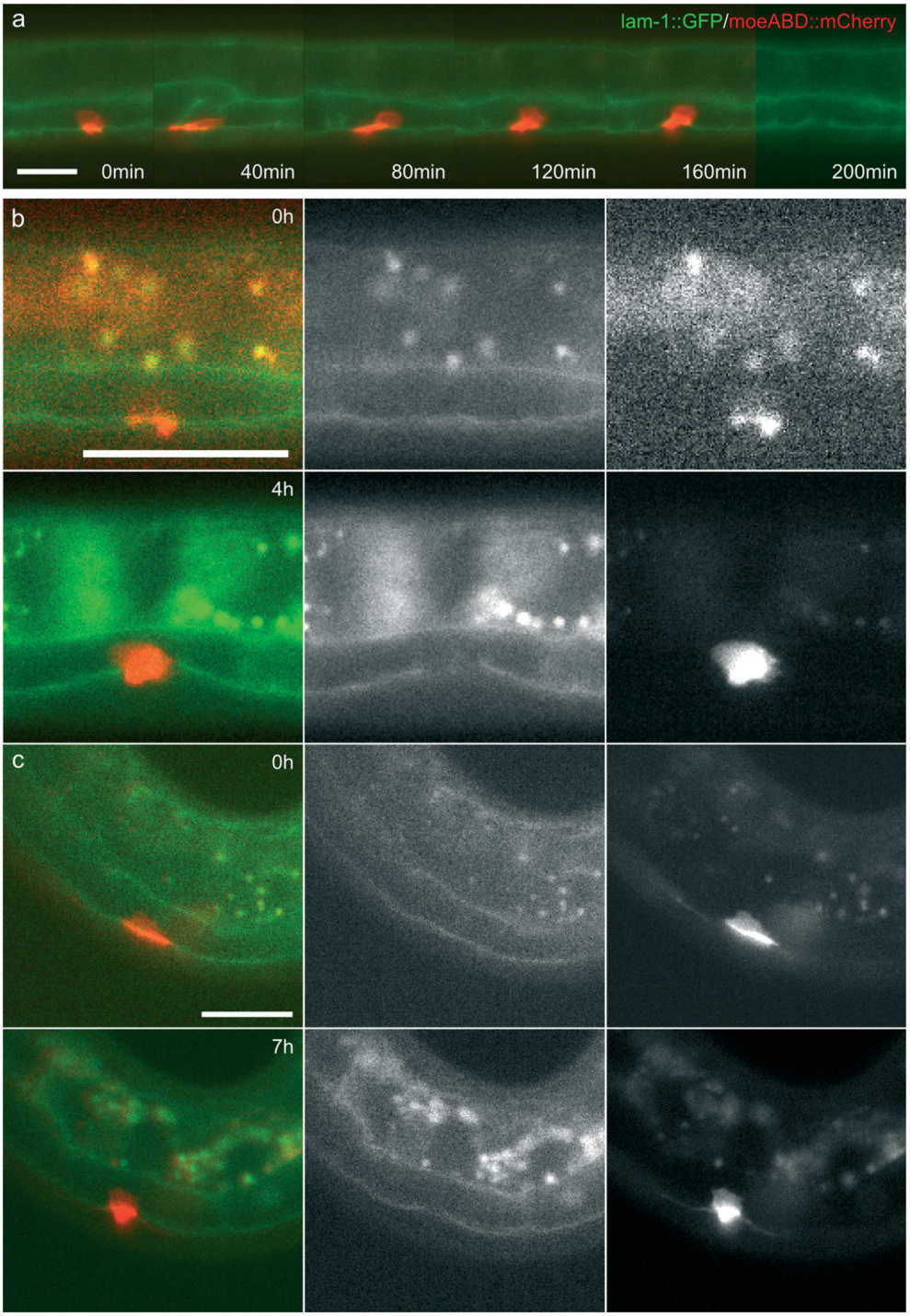

Fig. 5 AC invasion on-chip. (a) Time series of AC invasion in an L3 larva on-chip. During the time series the AC shows the typical elongation (40 min), followed by the formation of the lumen and the disruption of the basement membrane (at 120 min, at 200 min only GFP is shown). (b) AC invasion on-chip. The opening in the basement membrane and the lumen are clearly visible after 4 h and appear more pronounced on-chip, indicating gentler immobilization. Image quality on chip is comparable to the standard immobilization on pads. (c) AC invasion on agar pads. The opening in the basement membrane and the lumen are visible after 7 h. Development both on pads as well as on-chip arrests at the L3/L4 molt. Images were acquired using a 60× water immersion objective (NA 1.2) and an image splitter, simultaneously acquiring mCherry and GFP fluorescence. Scale bar 25 μm.

Conclusions

Herein we have presented a novel, easy to use microfluidic platform that combines both excellent immobilization performance and long-term worm viability. Optimal immobilization is achieved by carefully tailoring the geometry of a PDMS microfluidic device to the size and shape of the worms,

allowing unhindered egg laying and providing a constant supply of bacteria in suspension to ensure their adequate nourishment. Crucially, our approach minimizes stress, allowing all physiological processes to occur normally, while yielding immobilization performance comparable to conventionally used agar pads, without any of their shortcomings. Similarly, our platform does not pose any limitations on the imaging modalities used, offering excellent compatibility with all commonly used techniques. Data quality and resolution are solely limited by the microscope available.

We demonstrate the capabilities of our platform by studying three processes that, due to their sensitivity to conventional imaging procedures, are difficult to study dynamically *in vivo.* We were able to follow all three processes over extended periods of time, directly quantifying dynamics and timing at high resolution. Specifically, this has allowed measurement of germ cell migration and apoptosis directly by tracking individual cells over time, a feat not achieved to date. The fertilization rate and apoptotic rate are in good agreement with the experimentally found egg laying rate of 1 egg every 15 minutes and the apoptotic rates previously estimated by Gumienny *et al.*,[27] Fox *et al.*[30] and Jaramillo-Lambert *et al.*[31] We show that these rates can be highly variable even for worms maintained at identical conditions, highlighting the need to analyse such dynamic events *in vivo*, rather than through extrapolation from single time points.

We found that cell fluxes within the gonad are not homogenous with the majority of cells migrating either on the dorsal or ventral side. Apoptotic cell fates occur more frequently on the ventral side and non-apoptotic fates on the dorsal side. By tracking germ cells through a large section of the pachytene region we could show that the position within the gonad, far away from the turn, does not influence the cell fate decision later on, the effective decision only being made relatively close to the turn. Entrance to the turn from the ventral side is hindered due to the gonad's geometry, thus requiring cells on the ventral side to first migrate to the left and dorsal side before entering the turn. Determination of cell fate thus largely takes place during this stage with increased cell migration across the dorso-ventral axis. Competition for space and exposure to varying mechanical stresses may be involved in this process, so that it is conceivable that mechanical stress serves as a trigger for apoptosis. This is a hypothesis that will be investigated in the future. The live-imaging capability and subsequent possibility to track cells in time offered by our device, for the first time allowed us to gain insights into the complex cell migration and cell fate decision in the *C. elegans* gonad.

When applied to larval development, our platform enables more accurate analyses and with equivalent image quality when compared to conventional agar pads, again confirming its suitability for long-term imaging.[34] Moreover, the rapid and reliable occurrence of developmental processes in larval *C. elegans*, when compared to immobilization on agar pads, has significant implications for much of the developmental timing assumed to date, *e.g.* postembryonic cell lineage.

We envision that our platform will allow studies targeting many developmental processes in *C. elegans* larvae and adults that have to date been impossible to probe in real time. First, little is currently know about germ cell development, mitosis, meiosis and apoptosis, and we anticipate that our platform will help answer many of the unanswered questions. Similarly, our device can be used to study different aspects of development, such as nerve cord development, axon/dendrite outgrowth and Y cell transdifferentiation. Using the capabilities innate to the microfluidic system, the effects of chemical components, RNAi or dietary restriction on worm development and behaviour can also be probed at optimal resolution. Finally, the simplicity of our immobilization approach makes in amenable for integration into an automated platform for the screening of large worm populations, akin to previous work by Chung *et al.*[10,15] Likewise immobilization devices could be arranged in a parallel fashion such that multiple worms can be imaged at a time, or adapted for the immobilization of L1 and L2 stage larvae.

Conflicts of interest

The authors declare no conflicts of interest.

Acknowledgements

We would like to thank Dr Stavros Stavrakis for his help with microscopy and Ms Justina Rutkauskaite for her essential advise on bacteria preparation and cell density matching. This project was supported by Swiss National Science Foundation Grant CR2312-146328 and by the URPP Translational Cancer Research Fellowship.

Notes and references

1 M. Rodriguez, L. B. Snoek, M. De Bono and J. E. Kammenga, *Trends Genet.*, 2013, **29**, 367–374.
2 J. E. Sulston and H. R. Horvitz, *Dev. Biol.*, 1977, **56**, 110–156.
3 J. E. Sulston, E. Schierenberg, J. G. White and J. N. Thomson, *Dev. Biol.*, 1983, **100**, 64–119.
4 J. S. Simske and S. K. Kirn, *Nature*, 1995, **375**, 142–146.
5 M. C. Wong and J. E. Schwarzbauer, *Wiley Interdiscip. Rev.: Dev. Biol.*, 2012, **1**, 519–531.
6 Y. Chai, W. Li, G. Feng, Y. Yang, X. Wang and G. Ou, *Nat. Protoc.*, 2012, **7**, 2090–2102.
7 E. Kim, L. Sun, C. V. Gabel and C. Fang-Yen, *PLoS One*, 2013, **8**, 53419.
8 U. Wolke, E. A. Jezuit and J. R. Priess, *Development*, 2007, **134**, 2227–2236.
9 S. X. Guo, F. Bourgeois, T. Chokshi, N. J. Durr, M. A. Hilliard, N. Chronis and A. Ben-Yakar, *Nat. Methods*, 2008, **5**, 531–533.
10 K. Chung, M. M. Crane and H. Lu, *Nat. Methods*, 2008, **5**, 637–643.
11 T. V. Chokshi, A. Ben-Yakar and N. Chronis, *Lab Chip*, 2009, **9**, 151–157.

12 N. Chronis, M. Zimmer and C. J. Bargmann, *Nat. Methods*, 2007, **4**, 727–731.
13 S. E. Hulme, S. S. Shevkoplyas, J. Apfeld, W. Fontana and G. M. Whitesides, *Lab Chip*, 2007, **7**, 1515–1523.
14 C. B. Rohde, F. Zeng, R. Gonzalez-Rubio, M. Angel and M. F. Yanik, *Proc. Natl. Acad. Sci. U. S. A.*, 2007, **104**, 13891–13895.
15 M. M. Crane, J. N. Stirman, C. Y. Ou, P. T. Kurshan, J. M. Rehg, K. Shen and H. Lu, *Nat. Methods*, 2012, **9**, 977–980.
16 R. B. Kopito and E. Levine, *Lab Chip*, 2014, **14**, 764–770.
17 K. Chung, M. Zhan, J. Srinivasan, P. W. Sternberg, E. Gong, F. C. Schroeder and H. Lu, *Lab Chip*, 2011, **11**, 3689–3697.
18 N. Gritti, S. Kienle, O. Filina and J. S. Van Zon, *Nat. Commun.*, 2016, **7**, 12500.
19 S. E. Hulme, S. S. Shevkoplyas, A. P. McGuigan, J. Apfeld, W. Fontana and G. M. Whitesides, *Lab Chip*, 2010, **10**, 589–597.
20 J. Krajniak and H. Lu, *Lab Chip*, 2010, **10**, 1862–1868.
21 W. Keil, L. M. Kutscher, S. Shaham and E. D. Siggia, *Dev. Cell*, 2017, **40**, 202–214.
22 Y. Xia and G. M. Whitesides, *Annu. Rev. Mater. Sci.*, 1998, **28**, 153–184.
23 J. Chen and E. P. Caswell-Chen, *Nematology*, 2003, **5**, 641–645.
24 J. M. Adams, *Genes Dev.*, 2003, **17**, 2481–2495.
25 N. N. Danial and S. J. Korsmeyer, *Cell*, 2004, **116**, 205–219.
26 H. R. Horvitz, *ChemBioChem*, 2003, **4**, 697–711.
27 T. L. Gumienny, E. Lambie, E. Hartwieg, H. R. Horvitz and M. O. Hengartner, *Development*, 1999, **126**, 1011–1022.
28 J. Sulston, Cell Lineage, in *Cold Spring Harbor Monograph Archive*, 1998, vol. 17, pp. 123–155.
29 J. White, The Anatomy, in *Cold Spring Harbor Monograph Archive*, 1998, vol. 17, pp. 81–122.
30 P. M. Fox, V. E. Vought, M. Hanazawa, M. H. Lee, E. M. Maine and T. Schedl, *Development*, 2011, **138**, 2223–2234.
31 A. Jaramillo-Lambert, M. Ellefson, A. M. Villeneuve and J. Engebrecht, *Dev. Biol.*, 2007, **308**, 206–221.
32 R. Blelloch, C. Newman and J. Kimble, *Curr. Opin. Cell Biol.*, 1999, **11**, 608–613.
33 R. Lehmann, *Curr. Opin. Genet. Dev.*, 2001, **11**, 457–463.
34 E. J. Hagedorn, J. W. Ziel, M. A. Morrissey, L. M. Linden, Z. Wang, Q. Chi, S. A. Johnson and D. R. Sherwood, *J. Cell Biol.*, 2013, **201**, 903–913.
35 E. J. Hagedorn, L. C. Kelley, K. M. Naegeli, Z. Wang, Q. Chi and D. R. Sherwood, *J. Cell Biol.*, 2014, **204**, 1209–1218.
36 D. R. Sherwood and P. W. Sternberg, *Dev. Cell*, 2003, **5**, 21–31.
37 S. Lamouille, J. Xu and R. Derynck, *Nat. Rev. Mol. Cell Biol.*, 2014, **15**, 178–196.

